Biophysical Journal Volume 81 November 2001 2743–2751

Kinetics of Membrane Adhesion Mediated by Ligand–Receptor Interaction Studied with a Biomimetic System

Alexei Boulbitch, Zeno Guttenberg, and Erich Sackmann

Department für Biophysik E22, Technische Universität München, D-85747 Garching bei München, Germany

ABSTRACT We report the first measurement of the kinetics of adhesion of a single giant vesicle controlled by the competition between membrane–substrate interaction mediated by ligand–receptor interaction, gravitation, and Helfrich repulsion. To model the cell–tissue interaction, we doped the vesicles with lipid-coupled polymers (mimicking the glycocalix) and the reconstituted ligands selectively recognized by $\alpha_{IIb}\beta_3$ integrin-mediating specific attraction forces. The integrin was grafted on glass substrates to act as a target cell. The adhesion of the vesicle membrane to the integrin-covered surface starts with the spontaneous formation of a small (~200 nm) domain of tight adhesion, which then gradually grows until the whole adhesion area is in the state of tight adhesion. The time of adhesion varies from few tens of seconds to about one hour depending on the ligand and lipopolymer concentration. At small ligand concentrations, we observed the displacement ξ of the front of tight adhesion following the square root law $\xi \sim t^{1/2}$, whereas, at high concentrations, we found a linear law $\xi \sim t$. We show both experimentally and theoretically that the $t^{1/2}$-regime is dominated by diffusion of ligands, and the $\xi \sim t$-regime by the kinetics of ligands–receptors association.

INTRODUCTION

Cell adhesion is a nonequilibrium process that is controlled by the interplay of specific short-range attraction forces between receptor–ligand pairs and long-range repulsion forces. The latter are generated by stealth-like membrane proteins forming the glycocalix, such as the glycoprotein CD43 of leukocytes, which penetrates by ~40 nm into the extracellular space (Bongrand, 1999), or membrane-bound macromolecules of the extracellular matrix such as hyaluronic acid (Toole, 1990). In the case of erythrocyte, long-range repulsion forces may arise due to the undulational fluctuations of the membrane (the so-called Helfrich repulsion (Helfrich and Servuss, 1984)). One intriguing problem of cell adhesion concerns its kinetics, which appears to play a key role for cell recognition processes and depends both on the diffusibility of the receptors (Dustin et al., 1996) and the dynamics of expulsion of the repeller molecules from the contact zones (Bongrand, 1999).

In the previous model membrane studies, strong evidence was provided, that low receptor concentrations can lead to strong adhesion through the formation of tight adhesion domains composed of ligand–receptor pairs, which is reminiscent of the adhesion of cells on substrates through focal adhesion complexes (Smilenov et al., 1999). The adhesion-induced receptor segregation is a consequence of the competition between short-range attraction forces and long-range repulsion forces, which can result in a double minimum free energy of adhesion corresponding to states of tight and weak adhesion. The relative depth of two minima depends on the chemical potential (or osmotic pressure) of the repeller molecules of the nonadhering part of the vesicles membrane (comprising typically 80% of the total vesicle surface) and on gravity, because the solution inside the vesicle is denser than that outside (Guttenberg et al., 2001). The adhesion process is thus reminiscent of a first-order wetting transition (Bruinsma et al., 1999), or lateral phase separation (Komura and Andelman, 2000) and can thus be understood in terms of a nucleation and growth process. In a narrow region of the phase diagram at low receptor densities, the growth of spontaneously formed tight adhesion plaques stops, resulting in the coexistence of tight and weak adhesion zones, whereas, at high receptor–ligand pair content of the membrane, a homogeneous tight adhesion zone is formed (Guttenberg et al., 2001).

In the present paper, we study the adhesion of a single giant vesicle onto a solid substrate. This work is aimed to model the kinetics of cell adhesion. To mimic cell–tissue interaction, giant vesicles were used as test cells. They were composed of dimysistoylphosphatidylcholin and cholesterol (1:1 mixture) and were doped with lipid-anchored cyclic hexapeptides exhibiting an arginin glycine aspartate (RGD) motif and with phospholipid carrying a polyethyleneglycol (PEG) head groups of molecular weight 2000 to mimic the glycocalix. These PEG-lipopolymers act as repellers and help to suppress nonspecific van der Waals adhesion. Moreover, they promote formation of unilamellar vesicles. The RGD-ligand is selectively recognized by the integrin $\alpha_{IIb}\beta_3$ of blood platelets (Hu et al. 2000). This protein is physisorbed to glass substrates, which acts as target tissue with fixed receptors (as schematically shown in Fig. 1 *a*). Initially, vesicles were hovering over the substrate in a state of weak adhesion mediated by the interplay of gravitation and Helfrich repulsion. We then observed nucleation and growth of tight adhesion zones. Analysis of the displacement of the front of the tight adhesion region $\xi = \xi(t)$ at

Received for publication 24 April 2001 and in final form 30 July 2001.

Address reprint requests to A. Boulbitch, Dept. für Biophysik E22, Technische Universität München, James-Franck-St., D-85747 Garching bei München, Germany. Fax: +49-89-2891-2469; E-mail: aboulbit@physik.tu-muenchen.de.

0006-3495/01/11/2743/09 $2.00

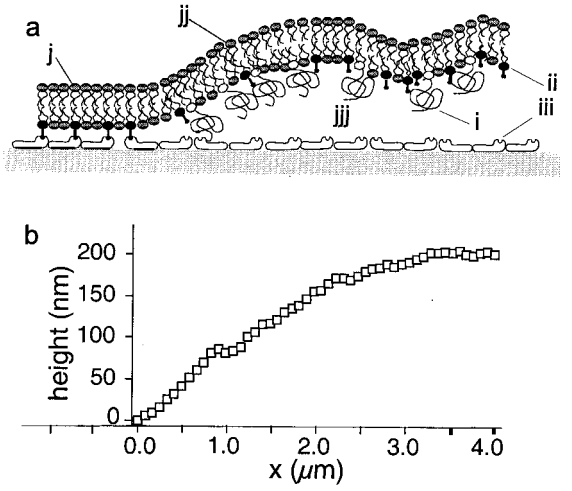

FIGURE 1 (*a*) Membrane at the substrate with two co-existing adhesion regions. *i*, The PEG lipo-polymers forming mushrooms model the mechanical effect of the cellular glycocalix; *ii*, the RGD ligands; *iii*, the receptors represented by protein integrin lying over the substrate; *j*, the area of the strong adhesion driven by the ligand–receptor interaction; *jj*, the region of the weak adhesion characterizing by the manifested height fluctuations; *jjj*, the volume enclosed between the membrane and the substrate. The water and PEG polymers contained in this volume take part in the energy dissipation during motion of the front of the strong adhesion. (*b*) Typical profile of the adhered membrane across the front in the region of the transition from the strongly to the weakly adhered state reconstructed by RICM.

small ligand concentrations has demonstrated the square root dependence on time $\xi \sim t^{1/2}$, whereas, at high concentrations, the front moves with a constant velocity $\xi \sim t$. We observed that the front velocity decreases exponentially with increasing concentration of PEG-lipids. We show theoretically that the square root regime of the front motion is dominated by the diffusion of the RGD-lipids, while the constant velocity regime is controlled by the ligand–receptor association reaction.

The paper is organized as follows. In the next section, we propose the theoretical approach describing the motion of the adhesion front. The following section describes materials and methods of our experiments. Then we describe the experimental results on the adhesion kinetics. Discussion of these results in the light of our theoretical approach is contained in the last section.

THEORETICAL DESCRIPTION OF THE MOTION OF THE ADHESION FRONT

Consider the motion of the front of the tight adhesion region (Fig. 1 *a*). According to our observations, we assume that it is dominated by two processes.

1. Ligands diffuse from the free membrane to the front. However, the diffusing ligands do not react with the receptors, because the weakly-bound part of the membrane is situated too far from the substrate covered by the receptors. The PEG molecules form mushrooms at the weakly bound membrane part the Flory radius of which is 3.5 nm and is larger than the length of the head group of the RGD ligand (2.2 nm). This prevents the ligand–receptor binding that could be mediated by the membrane fluctuation. Such a secondary nucleation process was observed only in a few cases.
2. In the close vicinity of the front (referred to as the "reaction zone") binding–unbinding reaction

$$\mathrm{L} + \mathrm{R} \rightleftarrows \mathrm{LR} \tag{1}$$

of the ligands (L) to the receptors (R) takes place. It is described by the equation

$$\frac{\partial c}{\partial t} = -k_+ c_{\mathrm{int}}(c - c_{\mathrm{eq}}) \tag{2}$$

(see Appendix A), where c is the surface number density of ligands, c_{eq} is its value in equilibrium with the ligand–receptor pairs: $c_{\mathrm{eq}} = k_- c_0 / k_+ c_{\mathrm{int}}$, where k_+ is the quasi-two-dimensional forward reaction rate, k_- is the dissociation rate, c_0 is the surface number density of the ligand–receptor pairs (Appendix A). Because $c_{\mathrm{int}} \approx c_0$, one finds $c_{\mathrm{eq}} \approx K_{\mathrm{d}} = k_-/k_+$.

At small values of the ligand concentration, the diffusion time τ_{d} is larger than the time of reaction τ_{r} and one finds the diffusion-dominated regime, whereas, at larger values of the ligand concentrations, the front motion is dominated by the kinetics of the reaction of ligands–receptors association.

The diffusion-dominated regime

Consider the front motion within a simple one-dimensional approximation. In other words, we assume that the front of the strong adhesion represents a straight line moving along the x axis, whose position we denote as $x = \xi(t)$. During its growth by a distance dx, the amount of bound ligand–receptor pairs, N, is increased by $dN = c_0 L dx$, where c_0 is the surface number density of the ligand–receptor pairs in the region of the strong adhesion and L is the front length. In contrast, if, during the time interval dt, the surface number density of the free ligands in the reaction zone (width b) decreases (and the concentration of the ligand–receptor pairs increases) by dc the surface number density of the ligand–receptor pairs increases by $dN = bLdc$. This yields the relation

$$c_0 \frac{\partial \xi}{\partial t} = b \frac{\partial c}{\partial t}. \tag{3}$$

In the diffusion-dominated regime, the chemical equilibrium is formed on the line $x = \xi$. However, the reaction takes place in the reaction zone representing a narrow band in the vicinity of the contact line. Therefore, the average surface density of ligands in the reaction zone $c = c(x)$ can

be expanded in series in terms of $x \leq b$ up to the first order. This yields the average value of the surface concentration in the reaction zone: $c \approx K_d + bc'(\xi)/2$, where $c' \equiv \partial c/\partial x$. Taking Eqs. 2 and 3 into account, one finds the equation at the adhesion front

$$\frac{\partial \xi}{\partial t} = \frac{1}{2} k_+ b^2 c'(\xi). \tag{4}$$

The distribution of the surface density of the ligands is described by the diffusion equation

$$\frac{\partial c}{\partial t} = Dc'', \tag{5}$$

with the boundary conditions,

$$c(\xi) = K_d \quad c(\infty) = c_L, \tag{6}$$

where c_L is the surface density of ligands in the free membrane part far from the front, and we assume that c_L is known from the preparation procedure.

Eqs. 4–6 are reminiscent of the so-called Stefan problem (Tikhonov and Samarskii, 1963). Its solution has the form

$$c(t,x) = A + B \operatorname{erf}\left\{\frac{x}{2\sqrt{Dt}}\right\}, \tag{7}$$

with constants A and B. The solution, Eq. 7, is compatible with the boundary conditions, Eq. 6, only if

$$\xi = \alpha \sqrt{t}, \tag{8}$$

with a constant value of the parameter α. The constants A and B are expressed as

$$A = \frac{K_d - c_L \operatorname{erf}(\mu)}{1 - \operatorname{erf}(\mu)} \quad B = \frac{c_L - K_d}{1 - \operatorname{erf}(\mu)} > 0, \tag{9}$$

where $\operatorname{erf}(\mu) = 2\int_0^\mu \exp(-p^2)\, dp/\sqrt{\pi}$ and $\mu = \alpha/(2\sqrt{D})$. Substitution of Eqs. 7–9 into the equation of the boundary motion, Eq. 4, yields

$$\alpha \approx \frac{k_+ b^2 (c_L - K_d)}{\sqrt{\pi D}} \tag{10}$$

(see Appendix C). Eq. 8 represents the equation of motion of the front of the tight adhesion. In the following, we reefer it to as the square root regime of the front motion and the constant α as the constant of the square root regime.

Reaction-dominated regime of motion with a constant velocity

At a high concentration of ligands, their diffusion plays a negligible role, and the front motion is determined by the reaction Eq. 1 kinetics. Because the membrane–substrate distance increases rapidly with the distance from the adhesion front, the reaction is mediated by the membrane fluctuations that provide tight receptor–ligand contacts. In the vicinity of the rim, the membrane possesses a curvature. In this region, membrane bending inevitably results in its stretching (Boulbitch, 1998). Therefore, the softest mode of these fluctuations is related to the displacement of the front without any bending. The energy required for such a fluctuation takes the form

$$\Delta W = \Pi \Delta A, \tag{11}$$

where $\Pi = c_P k_B T$ is the lateral osmotic pressure difference of the repellers, c_P is the surface number density of the lipopolymers PEG, and ΔA is the area variation during the front displacement by x. The probability $P(x)$ of fluctuations at which the front displaces by x is $P(x) = c_P L \exp(-c_P L x)$. It obeys the condition $\int P(x)\, dx = 1$. The probability of fluctuations with $x \leq x_0$ is $\omega(x_0) = \int_0^{x_0} P(x)\, dx$. One finds $\omega(x) = \exp(-c_P L x)$. Consider a minimal fluctuation soft mode at which the reaction, Eq. 1, becomes possible. This fluctuation corresponds to the forward displacement of the front by the average distance of a half a size of the integrin molecule. In this case, the work per ligand is $\Pi A_{int}/2$. The forward reaction rate takes the form

$$k_+ = k_{0+} \exp(-c_P A_{int}/2), \tag{12}$$

where k_{0+} is the forward reaction rate in a system without the lipopolymers. The characteristic time τ_r of the reaction Eq. 1 described by Eq. 2 takes the form

$$\tau_r = \frac{\exp(c_P A_{int}/2)}{k_{0+} c_{int}}. \tag{13}$$

Reaction Eq. 1 takes place in the reaction zone representing a narrow (width b) band along the front. As soon as a large part of the receptors of the reaction zone form ligand pairs, the front propagates one step forward. The front velocity is expressed as

$$v = \frac{b}{\tau_r} = b k_{0+} c_{int} \exp(-c_P A_{int}/2), \tag{14}$$

independent of the concentration of ligands. The expression, Eq. 14, does not take into account that the repeller's surface density in the free membrane area increases with the propagation of the front. This is valid for values of the ratio of the adhesion area to the total area below 0.3, which is typical for our measurements. In the Appendix C, one can find a more detailed analysis of the validity of the linear Eq. 14.

MATERIALS AND METHODS

Giant vesicles were prepared from a 1:1 mixture of dimyristoylphosphatidylcholine (DMPC) and cholesterol, to which 1–5 mol% of PEG-lipopolymer (dimyristoyl-phosphatidylethanolamin with a polyethyleneglycol (PEG) headgroup of molecular weight 2000 purchased from Polar Lipids, Alabaster AL) was added (the purity was more than 99%). We also added

0.08–2 mol% of lipid-coupled cyclic hexapeptide containing a RGD sequence that is selectively recognized by the integrin $\alpha_{IIb}\beta_3$ receptor of blood platelets (Hu et al., 2000). These ligands were synthesized by the group of L. Moroder at the Max Planck Institute, Martinsried, Germany. Separate studies with surface plasmon resonance showed that the dissociation constant is $K_d \approx 1.1\ \mu$M, compared to the $K_d \approx 0.1\ \mu$M of the natural ligand fibrinogen (Huber et al., 1995). Integrin receptors were prepared from blood platelets, solubilized by Triton X100, and fixed on a clean glass substrate by physisorption during incubation. For this purpose, the Triton-solubilized integrin receptor was dissolved in Tris-buffer (20 mM Tris pH 7.25, 150 mM NaCl, 1 mM $MgCl_2$, 1 mM $CaCl_2$, 1 mM NaN_3, 0.01% Triton X100) to a concentration of 68 nM and the substrates were incubated in this solution for 1 h. This procedure leads to a homogenous protein monolayer with 40% active protein, as tested by total internal reflection fluorescence measurements. In a second step, the substrates were incubated in a solution of 3 weight% bovine serum albumin in HEPES buffer (10 mM HEPES pH 7.25, 100 mM NaCl, 1 mM $CaCl_2$, 1 mM NaN_3). After each incubation, the substrates were thoroughly washed with HEPES buffer. We assume that residual Triton is removed during this procedure because no appreciable shape changes or instabilities of the giant vesicles were observed.

The giant vesicles were prepared by swelling under an AC electric field following Dimitrov and Angelova (1988). The lipid mixture was therefore deposited by solvent evaporation onto glass slides covered by indium-tin oxide, and swelling occurred with the addition of 170 mM sucrose solution during 2 h under 10 Hz and 1 V amplitude. Because the molar fractions of PEG lipopolymers and lipid-coupled RGD ligands added to the chloroform solution of the lipids were $\leq$5%, it is reasonable to assume that the components are completely reconstituted in the vesicles. The efficiency of the reconstitution was further checked by differential calorimetry. We found broadening of the main transition peak with increasing RGD lipid concentration up to 7 mol%, which provides further evidence for the above conclusion. Due to the presence of the PEG-lipid, most vesicles were unilamellar, and the giant vesicles were stable for several hours.

By adjusting the receptor concentration in the buffer, we could control the receptor area density on the substrate. Nonspecific binding was suppressed not only by reconstitution of PEG-lipids but also by coating the substrate with BSA. As a result, no appreciable adhesion of the membrane onto the substrate mediated by nonspecific attractive forces was observed either in the absence of grafted integrins or after photochemical denaturation of the receptor.

We have observed adhesion of the vesicles by reflection interference contrast microscopy (RICM) (Rädler and Sackmann, 1993), which allowed us to reconstruct the surface profile of the adhering vesicles with ~0.3-μm lateral resolution and 5-nm resolution in the vertical direction up to a height of 1 μm.

RESULTS

Fig. 1 *b* shows the reconstruction of the membrane–substrate distance. In the dark region, this distance cannot be measured by the RICM technique. It can, however, be estimated to be ~6.5 nm corresponding to the thickness of the integrin film measured by AFM (Guttenberg et al., 2000). In the region of the weak adhesion, we measured the membrane–substrate distance to be ~200 nm by RICM (Fig. 1 *b*). The formation of nuclei cannot be observed directly because their diameter is smaller than the optical resolution of the microscope (~300 nm).

Figure 2 shows a typical scenario of the adhesion process of a giant RGD- and PEG-lipid containing vesicle on an integrin-covered substrate observed by RICM. Initially, the vesicle hovers over the surface. One observes the nucleation of a small domain of a tightly adhered state after a delay time of about one minute to half an hour depending on the ligand and lipopolymer content. The process is slowed down by high PEG- and low RGD concentrations. Nucleation usually starts in the vicinity of the edge of the adhesion area (Fig. 2 *b*). The region of the tight adhesion grows gradually (Fig. 2, *b–d*), expanding until the whole contact zone is tightly adhered. The time from the nucleation until the complete adhesion depends on the concentrations of ligands and receptors and varies from ~30 s for 2 mol% RGD to 1600 s at 0.08 mol% RGD (shown in Fig. 4). The rim of the plaque of the tight adhesion closest to the outer rim of the adhesion disc grows only slightly slower than the opposite side.

The growth process of the area of the adhesion disk has been measured by image processing of a stack of successive images taken at time intervals of 1 s. The time dependence of the area of the adhesion spot was determined with the help of the software NIH-Image (NIH, Bethesda MD) starting from a minimum size of 1-μm diameter. Because the zones of the tight adhesion usually have an approximately circular shape (Fig. 2, *b–d*), the average displacement of the adhesion front can be determined as $\xi(t) = \{A(t)/\pi\}^{1/2}$. The time evolution of the front position as a function of ligand concentration is shown in Fig. 3. Two regimes can be distinguished. In the regime of high RGD concentration, the front moves with a constant velocity (Fig. 2, *a–c*) until the disc of the tight adhesion reaches the rim of the membrane–substrate interface (Fig. 2 *d*), when the motion is slowed down and finally stops. This constant velocity regime $\xi \sim t$ is shown in Fig. 3, *a–c*. For low RGD concentration, the front motion obeys the square root law $\xi \sim \sqrt{t}$ (Fig. 3, *d* and *e*).

The cross-over between these two regimes lies in the RGD concentration range between 0.2 and 0.1 mol%, which corresponds to the RGD-lipid surface-number density about equal to that of the active physisorbed integrin molecules. The integrin density (1.7×10^{15} m^{-2}) was determined by a separate total internal reflection fluorescence measurement. Therefore, the condition of the excess RGD concentration is no longer fulfilled, and diffusion shows a stronger influence.

The influence of the PEG-concentration on the kinetics of the adhesion could only be investigated in the high RGD concentration regime, because strong adhesion at PEG contents of up to 5 mol% can only be reached for 2 mol% RGD. The concentrations 3 and 5 mol% of PEG-lipids correspond to the regime of the front motion with a constant velocity.

We fitted the graphs for 0.2, 0.1, and 0.08 mol% RGD in Fig. 3 with a square root function $\xi = \alpha\sqrt{t}$, and the parameter α is plotted against RGD concentration in Fig. 4 *a*, showing a linear dependence as described by Eq. 10. In Fig. 4 *b* we plot velocities of the adhesion front versus the PEG concentration for a regime of the motion with a constant velocity. For each data point, 2–3 different vesicles were evaluated. The variation of the velocity with the RGD

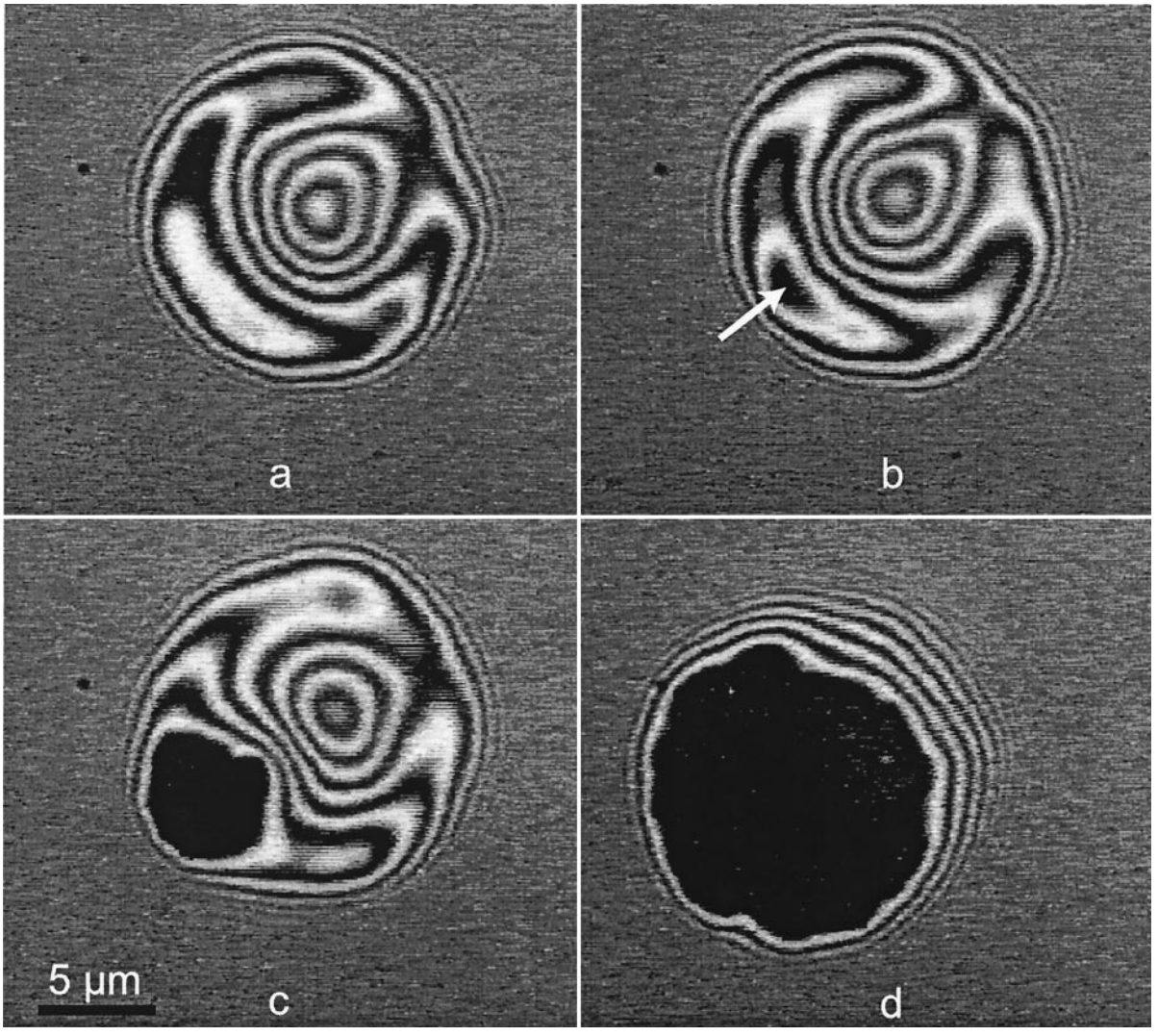

FIGURE 2 Adhesion area of a vesicle on the substrate. (*a*) The vesicle in the weakly adhered state. White and black rings represent the interference picture. (*b*) Nucleation of the state of the strong adhesion (*arrow*). (*c*, *d*) Different stages of the expansion of the strongly adhered state.

concentration can be fitted by an exponential function as predicted by Eq. 14, with the exponent $-c_P A_{int}/2 \approx -110n$, where $n = N_P/N_{lip}$, N_P is the number of the PEG repellers and N_{lip} is the number of lipids. For the constant velocity regime (corresponding to the situation shown in Fig. 3, *a–c*, the dependence of the front velocity on the RGD content is shown in Fig. 4 *c*. For the high concentrations of RGD-lipid (2 and 0.5 mol%), the velocity is approximately constant as predicted by Eq. 14. For the concentration 0.2 mol%, it decreases one order of magnitude and can therefore be interpreted as the onset of the cross-over from the reaction- to the diffusion-dominated regime.

The advancing front of the adhesion plaque is not, in all cases, a smooth line, but exhibits convex and concave regions (Fig. 5 *a*). If two of the convex regions ("arms") meet each other during the growth and join together (Fig. 5 *b*), the area behind this junction does not adhere strongly to the substrate, and a white spot (representing the region of the weak adhesion) remains trapped in the tightly adhered area. Such trapped regions of the weak adhesion appear both in the reaction- and diffusion-dominated regime and can be induced and stabilized by following mechanisms: 1) by inhomogeneities of the integrin layer, 2) by trapping of the PEG molecules that are unable to move out through the region of the tight adhesion, or 3) in the diffusion dominated regime the inclusion may be stabilized by the separation from the ligand reservoir.

DISCUSSION

Nucleation of the tight adhesion

Due to the high activation barrier separating the two minima, the initiation of the adhesion is expected to be a nucleation process. An important factor that controls the nucleation pro-

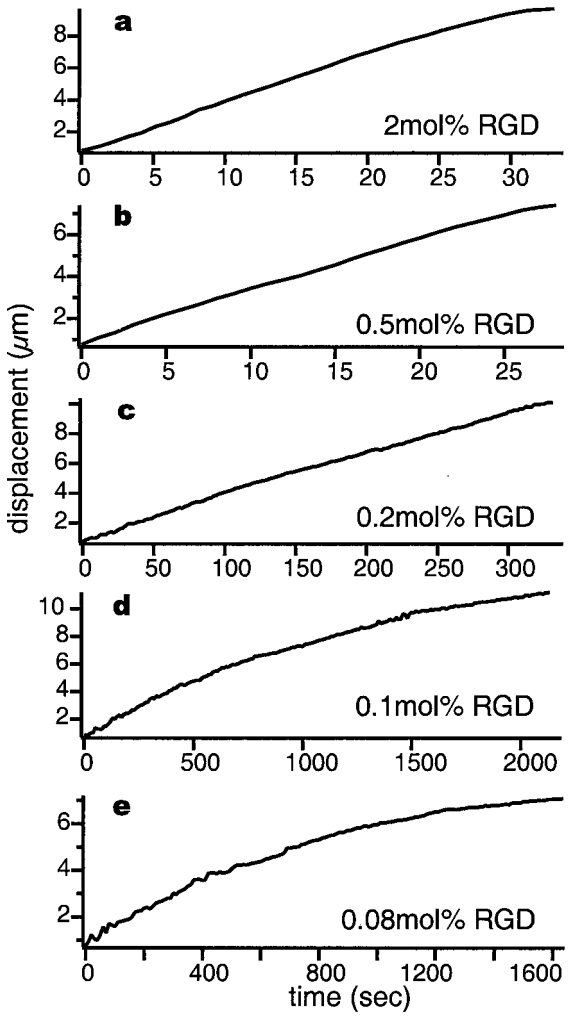

FIGURE 3 Displacement of the front of the tight adhesion versus time for different concentrations of ligands at 1 mol% PEG-lipid. The motion of the front was determined by measuring the area of tightly adhered plaque by the image processing. Assuming nearly circular area of the plaque, the front displacement can be calculated as $\xi(t) = \{A(t)/\pi\}^{1/2}$. For high RGD concentrations, the displacement increases linearly $\xi \sim t$ almost up to the end of the adhesion zone (*a*, *b*). For the lower ligand concentrations, (*d*, *e*), the front displacement exhibits a square-root regime $\xi \sim t^{1/2}$. (*c*) The cross-over state between the two regimes.

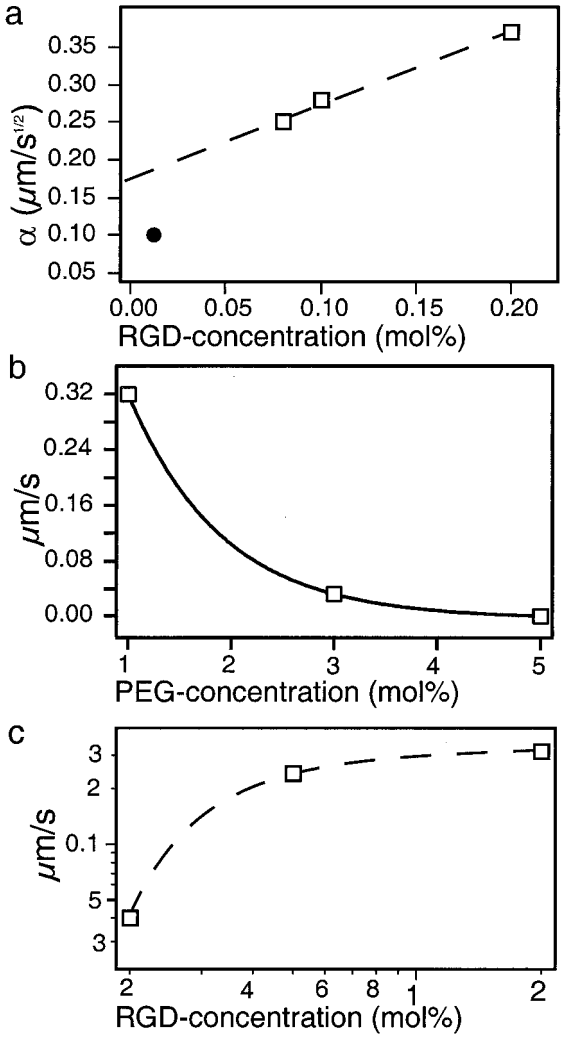

FIGURE 4 (*a*) The square root regime constant α as the function of RGD concentration obtained by fitting the displacement curves (*c*, *d*, *e*) shown in Fig. 3. The black circle represents α obtained using the data reported in Park et al. (1990). The dashed line shows the linear fit. (*b*) The front displacement versus the PEG concentration in the regime of the steady motion (corresponding to that shown in Fig. 3 *a*) at 2 mol% RGD. The solid line shows the exponential fit. (*c*) The displacement (*a*–*c*) shown in Fig. 3 where fitted with a linear function. The slopes were plotted against the RGD-lipid concentration. For the high RGD contents (*a*, *b*) the speed is nearly independent of the ligand concentration as expected from the theory for the reaction-dominated regime. The reduction of the speed for one order of magnitude for 0.2 mol% RGD-lipid represents the onset of the diffusion-controlled regime.

cess is the local elastic distortion of the membrane at the boundary region between tight and weak adhesion. Such a distortion takes place over a distance, *d*, that is about equal to the membrane persistence length with $d \sim 10^{-7}$–10^{-6} m (Guttenberg et al., 2001) comparable to the profile shown in Fig. 1 *b*. The form of the (double-well) potential (Bruinsma et al., 1999) defining the membrane shape in this case is unknown. This does not allow us to calculate the membrane profile. However, nucleation can be roughly described in terms of a model reminiscent of the theory of a first-order transition. The nucleation energy F is given by

$$F = -\pi r^2 \epsilon_{\mathrm{adh}} + 2\pi r T, \tag{15}$$

where r is the nucleus radius, ϵ_{adh} is the adhesion energy, T is the line tension of the nucleus rim (Bruinsma, 1996). Minimization of F with respect to r yields the relation between these parameters and the critical radius value r_c,

$$T = \epsilon_{\mathrm{adh}} r_c. \tag{16}$$

Making use of the minimal size of nuclei (close to the resolution limit of the microscope, 300 nm) that we observe, $r_c \sim 150$ nm, and our previous measurements, $\epsilon_{\mathrm{adh}} \sim 10^{-5}$

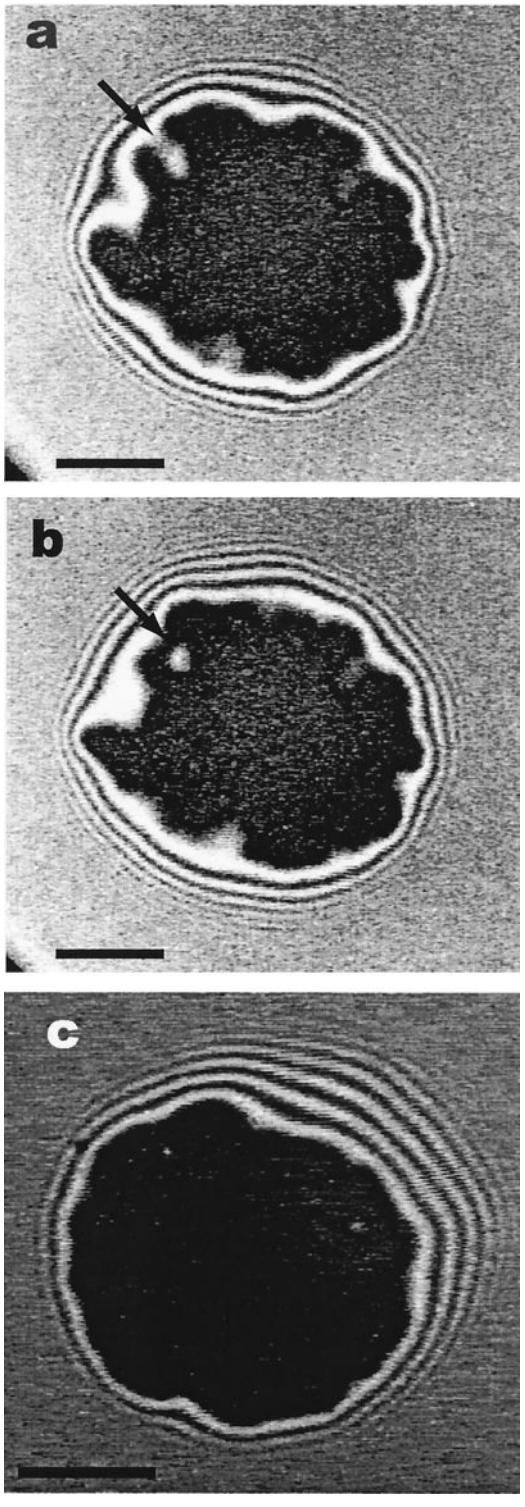

FIGURE 5 The front exhibits concave and convex regions in the square-root regime of motion (*a*, *b*), but is relatively smooth in the regime of motion with a constant velocity. (*a*, *b*) Formation of a small region of a weak adhesion (inclusion) trapped in the domain of the tight adhesion. (*a*) The inclusion formation begins with growing of two "arms" forming an invagination of the weakly adhered membrane (*arrow*). (*b*) Closing of the arms results in the trapping of the inclusion. Two successive images (*a*) and (*b*) are separated by one second. The adhering vesicle contains 0.08 mol% RGD- and 1 mol% PEG-lipid. The bars in the left lower corner of the images represent 5 μm.

J/m^2 (Guttenberg et al., 2001), one finds $T \sim 10^{-12}$ J/m. In contrast, the rim energy can be estimated as

$$T \sim \frac{\kappa}{2}\left(\frac{\partial^2 z}{\partial x^2}\right)^2 d, \tag{17}$$

where κ is the membrane-bending modulus and $z = z(x)$ describes the membrane profile. The expression $\kappa(z'')^2/2$ represents the membrane-bending energy per unit area stored in the rim, and d is the rim width. Making use the boundary conditions describing adhesion (Landau and Lifshitz, 1959; Seifert and Lipowsky, 1990; Seifert, 1991) and the rim size $d \sim 10^{-7}$ m, one finds the same estimate for the rim tension, T.

Characteristic times

The diffusion characteristic time can be estimated as

$$\tau_d \sim (Dc_L)^{-1}. \tag{18}$$

Assuming the concentration value $c_L = 0.1$ mol% $\sim 10^{15}$ m^{-2}, with which we observed the square-root regime (Fig. 3, *e* and *d*) and the diffusion constant $D \sim 10^{-12}$ m^2/s (Albersdörfer et al., 1997) one finds $\tau_d \sim 10^{-3}$ s.

The reaction time, Eq. 13, at small repeller concentration is

$$\tau_r = \frac{d_r}{\gamma k_+^{(3D)} c_{int}} \tag{19}$$

(see Appendix A for the description of the parameters and details). The square-root regime of the front motion $\xi \sim t^{1/2}$ takes place, if $\tau_r < \tau_d$. At $\tau_r \sim \tau_d$, one finds a cross-over regime. Estimating $d_r \sim 10^{-8}$ m, the condition of the cross-over regime yields $\gamma \sim 100$.

Front motion

In the square-root regime, our approach predicts that the motion constant α linearly depends on the concentration of ligands c_L, Eq. 10. This fits our observations (Fig. 4 *a*). Fitting its slope, we can estimate the width b of the reaction zone,

$$b^2 = \frac{d_r\sqrt{\pi D}}{\gamma k_+^{(3D)}}\frac{\partial \alpha}{\partial c_L}. \tag{20}$$

Making use the above estimates, one finds $b \approx 3 \times 10^{-8}$ m, which is about the size of an integrin molecule.

At $c_L \geq 1$ mol%, one finds $\tau_r \gg \tau_d$. This corresponds to the constant-velocity regime of the front motion $\xi \sim t$. Denoting $n = N_P/N_{lip}$, where N_P is the number of the PEG repellers, and N_{lip} is the number of lipids, one finds the exponent Eq. 14,

$$a = \frac{c_P A_{int}}{2} = \frac{A_{int}}{2A_{lip}}\, n, \tag{21}$$

where A_{lip} is the area per lipid $A_{lip} \approx 6 \times 10^{-19}$ m^2. Using the value $A_{int} \approx 2.0 \times 10^{-16}$ m^2 (Hynes, 1992) one finds $a/n \sim 167$, which is close to the value $a/n \sim 110$, which we obtained by fitting the dependence of the front velocity on the PEG concentration (Fig. 4 *b*). Substituting the above values into Eq. 14 and taking into account that not more than 40% of integrins are active, one finds $v \sim 10^{-6}$ m/s which reasonably fits to our observations.

Other dissipative processes

The processes of diffusion of ligands and their reaction with the receptors is not the only dissipative processes occurring during adhesion. Motion of the front enforces water to move out of the space between the membrane and the substrate. The PEG-lipids are pushed out from the tight adhesion area into the region of the weakly bound and free membrane. The motion of the mushroom-like PEG-lipids dissipate some energy. One can show that the contributions of these processes are smaller than those considered above. In contrast, neglecting these phenomena in our approach results in the underestimation of the dissipation. Therefore, the calculated value of the front velocity ($v \sim 10^{-6}$ m/s) is larger than the experimentally measured ($v \approx 0.3 \times 10^{-6}$ m/s).

Motion of cells

The surface concentration of ligands on the outer membrane of living cells lies in the range of 10^{14} m^{-2} (Bruinsma et al., 1999). The smallest RGD concentration for which we observed the tight adhesion used was $C_{min} \approx 0.08$ mol%. Because the area per lipid molecule is 60 Å^2, the RGD-lipids surface number density is $c \approx 6.6 \times 10^{14}$ m^{-2}, somewhat higher than the above value. For 0.01 mol% RGD the vesicles adhere only weakly to the surface during several hours of observation. The higher efficiency of cell adhesion may be due to the higher binding constants of the natural proteins, the coupling of the cytoskeleton to the receptor or a different thickness and density of the repelling polymer layer.

The speed of cell adhesion was measured for blood platelets on fibrinogen physisorbed on glass functionalized by RGD-ligands (Park et al., 1990). The platelet membrane contains the same type of integrin molecules as those used in our experiments, whereas, the corresponding RGD sequence one finds on the fibrinogen molecules. Although the dispositions of ligands and receptors are opposite with respect to that in our system, the specific bond ($\alpha_{IIb}\beta_3$-RGD) is the same. For a saturated value of the surface concentration of fibrinogen Park et al. (1990) observed that the tightly adhered area increased linearly with time $A(t) \sim t$ (which corresponds to the square-root regime of the front motion $\xi \sim t^{1/2}$) until about ⅔ of the adhesion area was strongly bound, and, after that, the area increase was observed to slow down. The plaque of the tight adhesion was reported to have also an approximately circular shape (Park et al., 1990). Fitting the data reported by Park et al., we obtained the constant of the square-root regime $\alpha \approx 0.1$ μm/s$^{1/2}$. This is close to the value expected from a linear extrapolation of the data points measured in the diffusion-dominated regime of the vesicle adhesion (Fig. 4 *a*), if the cell surface ligand concentration is 10^{14} m^{-2} (as estimated by Bruinsma et al., 1999).

CONCLUDING REMARK

We studied the dynamics of the (gravity-mediated) adhesion of soft shells containing ligands (mimicking test cells) on planar, receptor-covered substrates (mimicking target cells), which is controlled by the competition between specific short-range attraction forces, long-range repulsive interaction including Helfrich force and steric interaction between lipopolymers mimicking the glycocalix of cells and gravitation. The shell–substrate interaction is described by a double minimum potential with activation barrier height determined by the chemical potential of repeller molecules in the nonadhering membrane. We show that the dynamics of adhesion can be understood in terms of nucleation and growth process associated with the transition of the membrane from the weak to the strong adhesion state. The nucleation is a consequence of the line tension arising at the rim of tight adhesion plaques due to the local bending of the membrane. Depending on the concentration of receptor–ligand pairs, we find two types of growth behavior of the zone of the tight adhesion. At high concentrations the front of the tight adhesion plaque propagates with constant velocity determined by the kinetics of the ligand–receptor formation. At low ligand densities, the growth is a diffusion-limited process and the front coordinate increases with time as $\xi \sim t^{1/2}$.

APPENDIX A

The kinetics of the reaction Eq. 1 taking place in three-dimensional (3D) space can be described as

$$\frac{\partial C}{\partial t} = -k'_+ C_{int}(C - C_{eq}), \qquad \text{(A1)}$$

where C is the molar concentration of ligands (with the dimension M = mol/l), C_{eq} is its equilibrium value, C_{int} is the molar concentration of integrin, and k'_+ is the bulk forward reaction rate (measured in M^{-1} s^{-1}).

The rates of ligand–receptor association and dissociation reactions taking place in two-dimensions were shown to be different from that in the three-dimensions (Bell, 1978). The situation in our case, however, differs from the purely two-dimensional (2D) one considered by Bell (1978), because although the diffusion is 2D, the reaction takes place only in a narrow zone, where the membrane comes close enough to the substrate. One can come to a 2D description of the reaction kinetics in this zone by the transformation $c = 6 \times 10^{26} \times C d_L$; $c_{eq} = 6 \times 10^{26} \times C_{eq} d_{RGD}$; c_{int}

$= 6 \times 10^{26} \times C_{int} d_r$, which relate the 3D molar concentrations C, C_{eq}, and C_{int} to the surface number densities c, c_{eq}, and c_{int} (measured in m^{-2}), and

$$k_+ = \frac{\gamma k_+^{(3D)}}{d_r}, \tag{A2}$$

where it is convenient to express the bulk forward rate (measured in $m^3 s^{-1}$) in terms of the relation $k_+^{(3D)} = 1.7 \times 10^{-27} \times k'_+$. Here $c_{int} = A_{int}^{-1}$, k_+ is the 2D forward reaction rate (with the dimension $m^2 s^{-1}$), d_L is the diameter of the RGD head-groups (representing the thickness of the corresponding layer), and d_r is the thickness of the layer in which the reaction takes place: $d_r \sim 10^{-9}$–10^{-8} m. The constant γ is a dimensionless geometric factor. It accounts for the fact that, in our experiments, ligands and receptors are oriented in a favorable way, whereas the 3D reaction rate is measured for unoriented molecules. Therefore, the association reaction takes place faster than should be expected from the 3D reaction rate. For the case of antigens and antibodies, the estimate $\gamma \sim 1$–10 was given in Bell (1978). With the above definitions, Eq. A1 yields the kinetic Eq. 2.

APPENDIX B

The value of the derivative of the surface density of ligands with respect to x at the front $x = \xi$ has the form

$$\left(\frac{\partial c}{\partial t}\right)_{x=\xi} = \frac{c_L - K_d}{\{1 - \mathrm{erf}(\mu)\}\sqrt{\pi D t}} \exp\{-\mu^2\}. \tag{B1}$$

Therefore, denoting $q = k_+ b^2 (c_L - K_d)/(2D\sqrt{\pi})$ and substituting Eqs. 7–9 into the equation of the boundary motion Eq. 4 yields

$$\mu = \frac{q \exp(-\mu^2)}{1 - \mathrm{erf}(\mu)}, \tag{B2}$$

which, yields $\mu = \mu(q)$ in an implicit form. For $q \ll 1$ valid for the case under consideration one obtains the approximate solution of this equation in a form Eq. 10.

APPENDIX C

To test the applicability of Eq. 14 and to clarify the influence of the decrease of the reservoir area, consider the dependence of the surface number density of the repellers on the position of the front,

$$c_P = \frac{c_{P0}}{1 - \xi L/A_{tot}}, \tag{C1}$$

where c_{P0} is the initial concentration of repellers, ξ is the front displacement, and A_{tot} is the total membrane area. The constant $\omega = \xi L/A_{tot}$ is the ratio of the strong adhesion area to the total area of the membrane with typical values $\omega < 0.3$. The equation of the front motion takes the form

$$\frac{\partial \xi}{\partial t} = v_0 \exp\left\{-\frac{c_{P0} A_{int}}{2(1 - \xi L/A_{tot})}\right\} \tag{C2}$$

where $v_0 = b k_+ c_{int}$. Integrating Eq. C2 one finds

$$\frac{2A_{tot} v_0}{c_{P0} A_{int} L} t = \mathrm{Ei}\left\{\frac{c_{P0} A_{int}}{2(1 - \xi L/A_{tot})}\right\} - \frac{2(1 - \xi L/A_{tot})}{c_{P0} A_{int}} \exp\{2(1 - \xi L/A_{tot})\} - \mathrm{Ei}\left\{\frac{c_{P0} A_{int}}{2}\right\} + \frac{2\exp(c_{P0} A_{int}/2)}{c_{P0} A_{int}}, \tag{C3}$$

which defines $\xi = \xi(t)$ in the implicit form. Here, $\mathrm{Ei}(x) = -\int_{-x}^{\infty} p^{-1} \exp(-p)\, dp$. One can prove that, at $\omega \leq 0.3$ the linear regime $\xi(t) \sim t$ is rather accurate.

REFERENCES

Albersdörfer, A., T. Feder, and E. Sackmann. 1997. Adhesion-induced domain formation by interplay of long-range repulsion and short-range attraction force: a model membrane study. *Biophys. J.* 73:245–257.

Bell, G. I. 1978. Models for the specific adhesion of cells to cells. *Science.* 200:618–627.

Bongrand, P. 1999. Ligand–receptor interaction. *Rep. Prog. Phys.* 62: 921–968.

Boulbitch, A. A. 1998. Deflection of a cell membrane under application of a local force. *Phys. Rev. E.* 57:2123–2128.

Bruinsma, R. 1996. Adhesion and rolling of leukocytes: a physical model. *In* NATO ASI Series. Proc. NATO Advanced Institute on Physics of Biomaterials, Geilo, 1995. E. T. R. a. D. Sherrington, editor. Kluwer, Dordrecht, The Netherlands. 61.

Bruinsma, R., A. Behrisch, and E. Sackmann. 1999. Adhesive switching of membranes: experiment and theory. *Phys. Rev. E.* 61:4253–4267.

Dimitrov, D. S., and M. I. Angelova. 1988. Lipid swelling and liposome formation mediated by electric fields. *Bioelectrochem. Bioenerg.* 253: 323–336.

Dustin, M. L., L. M. Ferguson, P. Y. Chan, T. A. Springer, and D. E. Golan. 1996. Vizualization of CD2 interaction with LFA-3 and determination of the two-dimensional dissociation constant for adhesion receptors in a contact area. *J. Cell. Biol.* 132:465–477.

Guttenberg, Z., A. R. Bausch, B. Hu, R. Bruinsma, L. Moroder, and E. Sackmann. 2000. Measuring ligand–receptor unbinding with magnetic beads: molecular leverage. *Langmuir.* 16:8984–8993.

Guttenberg, Z., B. Lorz, E. Sackmann, and A. Boulbitch. 2001. First order transition between adhesion states in a system mimicking cell-tissue interaction. 2001. *Europhys. Lett.* 54:826–832.

Helfrich, W., and R. M. Servuss. 1984. Undulations, steric interaction and cohesion of fluid membranes. *Nuovo Cimento.* 3D:137–151.

Hu, B., D. Finsigner, K. Peter, Z. Guttenberg, M. Bärmann, H. Kessler, A. Escherich, L. Moroder, J. Böhm, W. Baumeister, S. Sui, and E. Sackmann. 2000. Intervesicle cross-linking with integrin $\alpha_{lib}\beta_3$ and cyclic-RGD-lipopeptide. A model of cell-adhesion process. *Biochemistry.* 39: 12284–12294.

Huber, W., J. Hurst, D. Schlatter, R. Barner, J. Hubscher, W. C. Kouns, and B. Steiner. 1995. Determination of kinetic constants for the interaction between the platelet glycoprotein IIb–IIIa and fibrinogen by means of surface plasmon resonance. *Eur. J. Biochem.* 227:647–656.

Hynes, R. O. 1992. Integrins: versatility, modulation, and signalling in cell adhesion. *Cell.* 69:11–25.

Komura, S., and D. Andelman. 2000. Adhesion-induced lateral phase separation in membranes. *Eur. Phys. J. E.* 3:259–271.

Landau, L. D., and E. M. Lifshitz. 1959. Theory of Elasticity. Pergamon Press, London. 51.

Park, K., F. W. Mao, and H. Park. 1990. Morphological characterization of surface-induced platelet activation. *Biomaterials.* 11:24–31.

Rädler, J., and E. Sackmann. 1993. Imaging optical thicknesses and separation distances of phospholipid vesicles at solid surfaces. *J. Phys. II (France).* 3:727–748.

Seifert, U. 1991. Adhesion of vesicles in two dimensions. *Phys. Rev. A.* 43:6803–6814.

Seifert, U., and R. Lipowsky. 1990. Adhesion of vesicles. *Phys. Rev. A.* 42:4768–4771.

Smilenov, L. B., A. Mikhailov, R. J. Pelham, E. E. Marcantonio, and G. G. Gundersen. 1999. Focal adhesion motility revealed in stationary fibroblasts. *Science.* 286:1172–1174.

Toole, B. P. 1990. Hyaluronan and its binding proteins, the hyaladherins. *Curr. Opin. Cell Biol.* 2:839–844.

Tikhonov, A. N., and A. A. Samarskii. 1963. Equations of Mathematical Physics. Pergamon Press, Oxford, U.K.